Astrocytes contribute to gamma oscillations and recognition memory

Hosuk Sean Lee[a,b,1], Andrea Ghetti[a,2], António Pinto-Duarte[c,d,e], Xin Wang[c], Gustavo Dziewczapolski[a], Francesco Galimi[f,g], Salvador Huitron-Resendiz[h], Juan C. Piña-Crespo[a,3], Amanda J. Roberts[h], Inder M. Verma[f], Terrence J. Sejnowski[c,i], and Stephen F. Heinemann[a,1]

[a]Molecular Neurobiology Laboratory, Salk Institute for Biological Studies, La Jolla, CA 92037; [c]Howard Hughes Medical Institute, Computational Neurobiology Laboratory, Salk Institute for Biological Studies, La Jolla, CA 92037; [f]Laboratory of Genetics, Salk Institute for Biological Studies, La Jolla, CA 92037; [h]Mouse Behavioral Assessment Core, The Scripps Research Institute, La Jolla, CA 92037; [b]Department of Life Sciences, Sogang University, Mapo-gu, Seoul 121-742, Republic of Korea; [d]Institute of Pharmacology and Neurosciences, Faculty of Medicine, University of Lisbon, 1649-028 Lisbon, Portugal; [e]Neurosciences Unit, Institute of Molecular Medicine, University of Lisbon, 1649-028 Lisbon, Portugal; [g]Department of Biomedical Sciences/Istituto Nazionale di Biostrutture e Biosistemi, University of Sassari Medical School, 07100 Sassari, Italy; and [i]Division of Biological Sciences, University of California, San Diego, La Jolla, CA 92093

Contributed by Stephen F. Heinemann, June 15, 2014 (sent for review March 10, 2014)

Glial cells are an integral part of functional communication in the brain. Here we show that astrocytes contribute to the fast dynamics of neural circuits that underlie normal cognitive behaviors. In particular, we found that the selective expression of tetanus neurotoxin (TeNT) in astrocytes significantly reduced the duration of carbachol-induced gamma oscillations in hippocampal slices. These data prompted us to develop a novel transgenic mouse model, specifically with inducible tetanus toxin expression in astrocytes. In this in vivo model, we found evidence of a marked decrease in electroencephalographic (EEG) power in the gamma frequency range in awake-behaving mice, whereas neuronal synaptic activity remained intact. The reduction in cortical gamma oscillations was accompanied by impaired behavioral performance in the novel object recognition test, whereas other forms of memory, including working memory and fear conditioning, remained unchanged. These results support a key role for gamma oscillations in recognition memory. Both EEG alterations and behavioral deficits in novel object recognition were reversed by suppression of tetanus toxin expression. These data reveal an unexpected role for astrocytes as essential contributors to information processing and cognitive behavior.

glia | electroencephalogram | network oscillation | gliotransmitter | glial fibrillary acidic protein

In the brain, the spatial and temporal coordination of networks of cells underlies both homeostatic and cognitive functions. Such synchronous activity gives rise to fluctuating local field potentials that can be recorded on the surface of the scalp by electroencephalography (EEG). Fast local field potential oscillations in the gamma frequency band (γ 25–80 Hz) have been closely correlated with learning, memory storage and retrieval, attention, and other cognitive or motor functions (1). In addition, in several neuropsychiatric disorders, gamma oscillations exhibit significant abnormalities that often correlate with the severity of the symptoms: a reduction in gamma oscillations is characteristic of the negative symptoms of schizophrenia, Alzheimer's disease, and autism, whereas the positive symptoms of schizophrenia, epilepsy, and attention-deficit hyperactivity disorder show increased gamma amplitudes (2). Nonetheless, the molecular mechanisms underlying these oscillations are poorly understood. Although the inhibitory interneurons (3, 4) and neuronal gap junction proteins Connexin-36 and -45 (5, 6) have all been shown to contribute to gamma oscillations, many of the molecular, cellular, and network mechanistic details underlying oscillations still remain undefined. Furthermore, the role of oscillations in brain function and behavior has yet to be fully clarified.

In the present work, we have moved away from the traditional focus of network oscillation research, namely neurons, and have instead investigated the consequences of a functional manipulation of astrocytes on network function and animal behavior. The role of astrocytes in maintaining the brain's energy balance and providing metabolic support to neurons is well established. In addition, in recent years many molecular commonalities have been uncovered between neurons and astrocytes that point to the possibility of a more direct involvement of astrocytes in information processing in the brain. For example, astrocytes express a variety of neurotransmitter receptors, respond to neuronal activation, and release chemical transmitters (termed "gliotransmitters") following intracellular calcium elevation (7–11). Although these newly discovered properties have been independently confirmed by several groups, their functional significance remains a matter of debate (12). Investigations aimed at manipulating transmitter-mediated communication between astrocytes and neurons have resulted in inconsistent findings in regard to synaptic function, synaptic plasticity, and behavior (13, 14). Some of these discrepancies are probably due to the variety of approaches used to alter astrocytic function as well as differences in physiological and behavioral readouts. Given the extensive array of shared molecular components, it is indeed difficult to specifically alter the physiology of astrocytes without, at the same time, directly impacting neuronal function.

Significance

Astrocytes are well placed to modulate neural activity. However, the functions typically attributed to astrocytes are associated with a temporal dimension significantly slower than the timescale of synaptic transmission of neurons. Consequently, it has been assumed that astrocytes do not play a major role in modulating fast neural network dynamics known to underlie cognitive behavior. By creating a transgenic mouse in which vesicular release from astrocytes can be reversibly blocked, we found that astrocytes are necessary for novel object recognition behavior and to maintain functional gamma oscillations both in vitro and in awake-behaving animals. Our findings reveal an unexpected role for astrocytes in neural information processing and cognition.

We conducted our experiments in transfected brain slices and in an inducible mouse model with temporally controlled and cell-specific expression of tetanus neurotoxin (TeNT), which we developed for this study. Our results uncover an unsuspected role for glial cells in neuronal network gamma oscillations and demonstrate their contribution to shaping higher brain functions and behavioral patterns.

Results

Transient Elevations in Intracellular Calcium Concentration in Astrocytes Precede the Onset of Oscillatory Activity.

Synchronized fast neuronal oscillations in the beta (β, 12–20 Hz) and gamma (γ, 25–60 Hz) ranges have been described in association with perceptual and cognitive activities (15, 16). Neuronal oscillations can be induced by a variety of protocols (17, 18) and have been extensively studied in vitro, especially in hippocampal slices. In this work, we have used cholinergic agonist carbachol (CCH) to induce oscillations in hippocampal slices. It has previously been shown that carbachol induces gamma oscillations in hippocampal slices by recruiting coordinated excitatory and inhibitory transmission in neural circuits (17). Using simultaneous imaging of intracellular calcium dynamics in astrocytes, loaded with the calcium sensor Fura-2 AM, and recording of field potentials in brain slices, we observed a temporal correlation between intracellular calcium elevations in astrocytes and field oscillatory activity ($n = 6$) (Fig. 1 B and C). The onset of the calcium response in astrocytes preceded the start of the oscillations by 5.3 ± 2.4 s (mean ± SEM). The traces in Fig. 1B were taken from Fura-2–loaded cells, which were confirmed to be astrocytes at the end of the experiment by postfixation immune-labeling with anti-GFAP antibodies (Fig. 1A). This correlation prompted further investigations aimed at establishing whether astrocytic calcium responses were necessary for neural oscillations, or simply an epiphenomenon.

Tetanus Toxin Expression in Cultured Astrocytes Disrupted Cell-to-Cell Signaling.

Because intracellular calcium elevations have been reported to be sufficient to induce glutamate release from astrocytes (19–21), we hypothesized that astrocytes might contribute to network oscillations by affecting the overall actions of glutamate and by modulating the excitability of the neuronal network. To investigate this possibility, we took advantage of the sensitivity of astrocytic calcium-dependent vesicular release to clostridial toxins (TeNT) (20, 22) and generated a genetic system capable of targeting TeNT expression to astrocytes. A synthetic gene coding for the TeNT catalytic domain (TeNT light chain, TeNT-LC) (23) was fused with the gene for green fluorescent protein (TeNT$^{\Delta 1}$-GFP; *Methods*) to track toxin expression. Both wild-type and GFP-fused toxins can efficiently cleave synaptobrevin2, thereby preventing vesicle release (24).

We verified the ability of TeNT$^{\Delta 1}$-GFP to inhibit glutamate release from astrocytes by using human embryonic kidney (HEK) cells made responsive to glutamate by the expression of the NMDA receptor subunits NR1 and NR2B (HEK-NMDA) (25, 26) (Fig. 2 A–E). These HEK-NMDA cells were plated on top of primary astrocyte cultures that had been transfected with either GFP (Fig. 2 A–C) or TeNT$^{\Delta 1}$-GFP cDNAs (Fig. 2 D and E). Thus, in this preparation, HEK-NMDA cells were able to detect glutamate released from astrocytes. Mechanical stimulation of untransfected astrocytes, or astrocytes transfected with GFP cDNA, induced a calcium response in all HEK-NMDA cells located within a 150-μm radius from the stimulation site ($\Delta F/F = 0.3 \pm 0.08$, mean ± SEM; $n = 21$ cells from three cultures) (Fig. 2B). Note that CCH could not be used in place of mechanical stimulation in these experiments because it also directly induced elevated calcium levels in HEK cells. Calcium responses in HEK-NMDA cells following mechanical stimulation of astrocytes were completely abolished by the NMDA receptor-antagonist APV (50 μM) ($n = 15$ cells from three cultures) (Fig. 2C).

In contrast, when astrocytes were transfected with TeNT$^{\Delta 1}$-GFP, mechanical stimulation did not result in a response in HEK-NMDA cells ($n = 16$ cells from three cultures) (Fig. 2E), presumably due to the impairment of vesicular release in astrocytes expressing the toxin. These results were consistent with previous reports (20, 21, 27, 28) and validated the sensitivity of astrocytic vesicular release to tetanus toxin block.

In Brain Slices, Astrocytic Expression of Tetanus Toxin Blocked Glutamate Release Without Interrupting Neuronal Synaptic Activity.

With the ultimate goal of expressing the TeNT$^{\Delta 1}$-GFP construct in astrocytes of brain slices, we engineered a lentiviral vector with the human astrocyte-specific promoter hGFAP (29) and a GFP-only control (Fig. 2F). We first infected primary cultures of astrocytes with the control virus (lenti-hGFAP-GFP) and then cultured HEK-NMDA cells on top as previously described. We found that the infection and subsequent GFP expression was successful, yet had no effect on astrocytic glutamate release (fluorescence changes in HEK cells within 150 μm from stimulation were the following: $\Delta F/F = 0.4 \pm 0.09$, mean ± SEM; $n = 8$ cells from three cultures) (Fig. 2 G and H). In contrast, infection with lenti-hGFAP-TeNT$^{\Delta 1}$-GFP effectively blocked glutamate release from astrocytes by the same measure ($n = 12$ cells from three cultures) (Fig. 2 I and J).
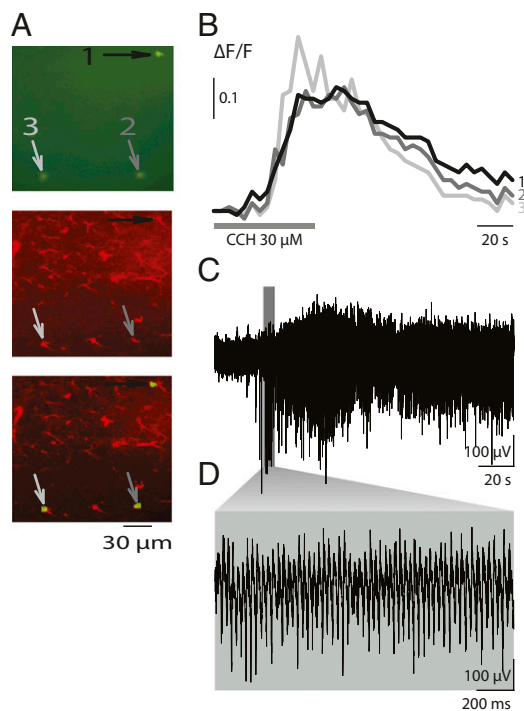
Fig. 1. Intracellular calcium responses precede carbachol-induced oscillations. (A) Immunofluorescence-based profiling of the three cells imaged in B. (Top) Fura-2–loaded cells (white arrows) visualized using a 380-nm excitation wavelength. (Middle) The slice was fixed and immunostained using a rabbit anti-GFAP antibody. (Bottom) The merge of the Left and Center panels shows that the Fura-2–loaded cells were GFAP-positive astrocytes. To minimize neuronal loading, short Fura-2–loading time was used, and consequently only a few cells were loaded with the calcium dye. (B) Example traces of intracellular calcium dynamics in three astrocytes from stratum radiatum of the CA3 area following carbachol treatment (CCH). (C) Extracellular field potential from the pyramidal cell layer of the CA3 area recorded simultaneously with the calcium imaging shown in B. Note that the onset of the calcium response preceded the start of the oscillations. (D) Gamma oscillations from recording in C shown on expanded time scale.
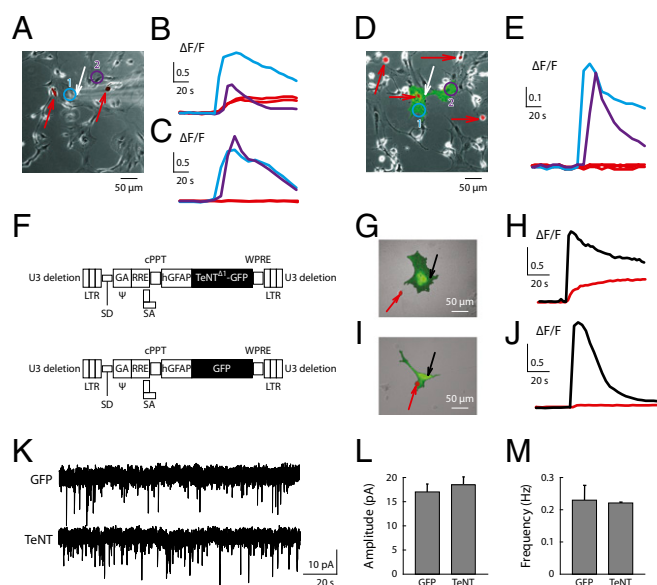
Fig. 2. Tetanus toxin expression in astrocytes eliminated the release of glutamate but did not significantly modify synaptic activity. The glutamate detectors (HEK-NMDA), the HEK cells with NR1 and NR2B, were seeded on top of primary astrocyte culture (*A*), and the HEK-NMDA cell responses to mechanical stimulation of astrocytes were measured using a fluorescent calcium indicator. (*A*) Merged bright-field and dsRed channel images. Transfected HEK cells are visualized by virtue of dsRed protein expression (red arrows). White arrow is the stimulation site. Numbered circles are astrocytes where the intracellular calcium dynamics were monitored. (*B*) Intracellular calcium concentration in astrocytes (blue and purple traces) and HEK-NMDA cells (red traces) following mechanical stimulation. (*C*) The experiment described in *A* and *B* was repeated in the presence of 50 μM AP-5. (*D* and *E*) Intracellular calcium concentration following transfection of astrocytes with TeNT$^{\Delta1}$-GFP cDNA. TeNT$^{\Delta1}$-GFP–transfected cells were visible with green fluorescent color (*D*); blue and purple traces are the astrocytes response to mechanical stimulation, whereas the HEK-NMDA cells did not detect any extracellular glutamate (*E*, red traces). (*F*) Schematic representation of the lentiviral vector constructs used in this study. (*G* and *H*) Infection of astrocytes with lenti-GFP. Red arrow indicates HEK-NMDA cell. Black arrow indicates stimulation sites. Intracellular calcium concentration (*H*) in astrocytes (black trace) and HEK-NMDA cells (red trace) following mechanical stimulation of the astrocyte. (*I* and *J*) Infection of astrocytes with lenti-TeNT$^{\Delta1}$-GFP with HEK-NMDA. Note that HEK-NMDA did not detect glutamate from the astrocytes infected with TeNT$^{\Delta1}$-GFP. (*K*–*M*) Targeted expression of TeNT to astrocytes in slice cultures had no significant effect on synaptic activity. Traces show mEPSCs recorded from pyramidal neurons in the CA3 region infected with astrocyte-targeted lentivirus containing GFP (*K*, *Upper*) and TeNT$^{\Delta1}$-GFP (*K*, *Lower*). (*L*) Mean amplitude of mEPSCs was 17.03 ± 1.64 pA (*n* = 3) and 18.51 ± 1.67 pA (*n* = 3) for GFP and TeNT$^{\Delta1}$-GFP, respectively. (*M*) Mean frequency of mEPSCs was 0.23 ± 0.046 Hz (*n* = 3) and 0.22 ± 0.002 Hz (*n* = 3) for GFP and TeNT$^{\Delta1}$-GFP, respectively.

We next used the viral vectors in primary hippocampal slices and validated the targeting of expression to astrocytes. Using immunohistochemistry, we found that GFP expression colocalized with a marker for astrocytes (GFAP), but not with one for neurons (NeuN) (Fig. S1*A*). Additionally, field-excitatory postsynaptic potentials recorded from infected cultured slices, expressing GFP alone or TeNT$^{\Delta1}$-GFP, were indistinguishable from each other (Fig. S1 *B* and *C*), suggesting that this measure of neuronal function was intact. Finally, we studied synaptic activity by recording miniature excitatory postsynaptic currents (mEPSCs) and found that pyramidal neurons located in the region infected with the lentiviral vectors showed normal mEPSCs (Fig. 2 *K*–*M*), again indicating normal function in these cells. Taken together, these results suggest that, when vesicle fusion in astrocytes was blocked by TeNT$^{\Delta1}$-GFP in our model, neuronal

synaptic activity remained largely unaltered and that there was no leaky expression of tetanus toxin in neuronal cells.

Blockade of Astrocytic Vesicular Release Shortened the Duration of Carbachol-Induced Gamma Oscillations in Vitro. Next we asked whether TeNT$^{\Delta1}$-GFP expression in astrocytes affected the neurophysiology of hippocampal slices. We first looked at network oscillations in slices that had been maintained in culture for at least 5 d and were either uninfected or infected with our control lenti-GFP (Fig. 3*A*). Bath application of carbachol (30–50 μM) induced fast gamma and beta oscillations (Fig. 3 *B* and *E*), similar to what has previously been reported in acute hippocampal slices (17, 18). However, when slices were infected with lenti-TeNT$^{\Delta1}$-GFP, carbachol induced only short-lasting gamma oscillations (Fig. 3*C*). The duration of gamma oscillations in uninfected and lenti-GFP–infected slices was 1.9 ± 0.4 s (mean ± SEM; *n* = 9) and 1.7 ± 0.2 s (mean ± SEM; *n* = 12), respectively. In contrast, in lenti-TeNT$^{\Delta1}$-GFP–infected slices, the duration of carbachol-induced gamma oscillations was reduced to 0.3 ± 0.07 s (mean ± SEM; *n* = 16) (Fig. 3*F*, F1). Other parameters of gamma oscillations (number of events, amplitude, and peak oscillation frequency) were not sensitive to toxin expression (Fig. 3*F*, F2–F4). Additionally, no alteration was observed in beta oscillations (Fig. 3*F*, F5–F8), suggesting that the effect of TeNT$^{\Delta1}$-GFP expression was specific to oscillations in the gamma frequency range. Next, using intracellular recordings, we measured the effect of astrocyte-specific TeNT expression on the depolarization of pyramidal cells induced by carbachol. In cultured slices infected with lenti-GFP, carbachol application resulted in large depolarizations of pyramidal neurons (18 ± 5 mV, mean ± SEM; *n* = 6), whereas expression of lenti-TeNT$^{\Delta1}$-GFP resulted in smaller carbachol-dependent depolarizations (6 ± 1 mV, mean ± SEM; *n* = 7; *P* = 0.02, Student's *t* test) (Fig. S2).

To eliminate the possibility that interslice variation caused some of the differences observed between control and lenti-TeNT$^{\Delta1}$-GFP–infected slices, we infected some slices (*n* = 4) with a limited amount of lenti-TeNT$^{\Delta1}$-GFP and restricted the infection to one small region. This allowed an internally controlled comparison of oscillatory behaviors inside and outside the infected area within the same slice. The duration of gamma oscillations recorded within the infected area was, in all cases, significantly shorter than the duration of gamma oscillations recorded outside the infected region (Fig. 3*G*).

Glutamate Receptor Agonist AMPA Reversed the Disruption of Gamma Oscillations. To test whether the shortening of gamma oscillations in TeNT$^{\Delta1}$-GFP–infected slices involved the impaired release of glutamate from astrocytes, we determined whether the exogenous application of the glutamate receptor agonist AMPA could reverse the effect of the toxin. Low concentrations of AMPA (10–30 μM) by themselves did not induce oscillatory activity at any frequency when applied to the slices. However, when carbachol (30 μM) and AMPA (20 μM) were coapplied to the lenti-TeNT$^{\Delta1}$-GFP–infected slices, the duration of the gamma oscillations was restored to control values (2.1 ± 0.5, mean ± SEM; *n* = 8) (Fig. 3 *D* and *F*, F1). These results showed that the integrity of the neural circuits responsible for gamma oscillations was intact in slices with astrocytic TeNT$^{\Delta1}$-GFP expression and that the shortening of the oscillations was not due to secondary effects of viral infection or to toxin expression. Furthermore, these findings suggest that glutamate could be a glia-released factor responsible for extending the otherwise shortened duration of gamma oscillations.

Development of an Inducible Transgenic Mouse Model Allowing Temporal and Cell-Specific Control of TeNT Expression in Astrocytes. Next, to find out whether the findings of astrocyte-mediated modulation of gamma oscillations in vitro had any physiological
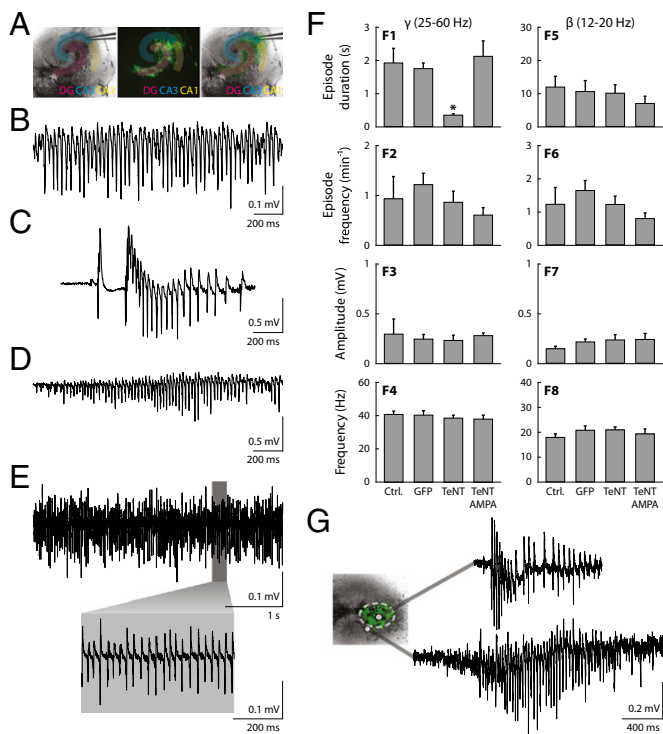
Fig. 3. Astrocyte-specific expression of tetanus toxin-disrupted hippocampal oscillatory activity in vitro. (*A*) Example of a cultured hippocampal slice. (*Left*) Bright-field image of the organotypic culture (the recording electrode is visible in the pyramidal layer of the CA3 area). (*Center*) GFP fluorescence emitted by the slice under UV-light illumination. (*Right*) Merged images. (*B*) Extracellular field recording showing a carbachol-induced gamma oscillations in a lenti-GFP–infected slice. (*C*) Oscillatory activity elicited by carbachol in a slice infected with lenti-TeNT$^{\Delta1}$-GFP. (*D*) Oscillatory activity induced by coapplication of carbachol (30 μM) and AMPA (30 μM) in the lenti-TeNT$^{\Delta1}$-GFP–infected slice. (*E*) Example trace of beta oscillations induced by charbachol in a lenti-GFP–infected slice. (*F*) Quantitative comparison parameters for the gamma (F1–F4) and beta (F5–F8) oscillations under different conditions. The different experimental conditions are indicated at the bottom (in all cases oscillations were induced by 30 μM carbachol): Ctrl, uninfected slices; GFP, slices infected with lenti-GFP; TeNT, slices infected with lenti-TeNT$^{\Delta1}$-GFP; TeNT/AMPA, oscillations induced by coapplication of carbachol (30 μM) and AMPA (30 μM) in slices infected with lenti-TeNT$^{\Delta1}$-GFP. Asterisk indicates $P < 0.05$ (ANOVA). (*G*) Shown in green is the region infected with lenti-TeNT$^{\Delta1}$-GFP. Field potentials recorded in the presence of 30 μM CCH from inside the infected area (*Upper* trace) or from outside the infected area (*Lower* trace).

or behavioral relevance in vivo, we generated a transgenic mouse line expressing TeNT in astrocytes. Our attempt to use the same lenti-GFAP-TeNT$^{\Delta1}$-GFP vector (Fig. 2*F*) for creating a transgenic mouse (30) failed to generate a mouse line with stable TeNT expression. We reasoned that the constitutive expression of the toxin in astrocytes might have been lethal to the animals.

We then developed a system in which astrocytic expression of TeNT$^{\Delta1}$-GFP could be controlled temporally. The transgene that we used contained two control elements: a tet-responsive element (TRE) promoter (31) that is active only when a tet-transactivator (tTA) is bound and a loxP-flanked transcriptional/translational STOP sequence (32), which prevented the expression of tetanus toxin unless it was excised by Cre recombinase. Hence, we created the transgene TRE-loxP-STOP-loxP-TeNT$^{\Delta1}$-GFP (for short, TRE-STOP-TeNT-GFP) and subsequently crossed it with the previously reported transgenic mouse lines GFAP-tTA (33) and GFAP-CreERt2 (34). CreERt2 is a fusion protein of the estrogen receptor to Cre recombinase that re-

moves the DNA segment between loxP sites (35, 36) when activated by tamoxifen (34, 37). Following excision of the STOP sequence, the TeNT$^{\Delta1}$-GFP gene is expressed in the presence of tTA without any further treatment and inhibited when tTA is deactivated by doxycycline (38). Because both tTA and CreERt2 are controlled by the astrocyte-specific GFAP promoter (human GFAP promoter) (39, 40), they are expressed exclusively in astrocytes. In a triple transgenic (TG) (3×TG) mouse carrying the TRE-STOP-TeNT-GFP, GFAP-tTA, and GFAP-CreERT2 constructs (Fig. 4*A*), therefore, TeNT would be (*i*) expressed exclusively in astrocytes, (*ii*) when tamoxifen was injected (3×TG-T) (Fig. 4*B*), and (*iii*) could be suppressed when mice were fed doxycycline (3×TG-T+D) (Fig. 4*C*). Only one of the five mouse lines generated showed efficient and restricted expression of the toxin that was dependent on tamoxifen for activation and doxycycline for suppression (mRNA detection was performed using RT-PCR; Fig. S3). We found that optimal treatment for inducing TeNT expression consisted of two daily i.p. injections of 100 μL tamoxifen (10 mg/mL), which resulted in maximal transcriptional levels of TeNT-GFP 2 d later.

Preserved Synaptic Responses in the Astrocyte-Specific TeNT-Inducible Mouse Model. To test if there were appreciable synaptic abnormalities in our inducible mouse model or leaky expression of TeNT in neurons, we recorded from acute brain slices prepared from transgenic animals. As shown in Fig. 5*A*, basal hippocampal synaptic transmission was not significantly affected by tamoxifen injection in 3×TG mice (3×TG-T, TeNT-expressing mice), compared with controls, 2×TG mice injected with tamoxifen (2xTG-T; GFAP-tTA and GFAP-CreERt2 only without TeNT transgene). Similarly, paired-pulse facilitation (Fig. 5*B*), synaptic fatigue (Fig. 5*C*), high-frequency–induced long-term potentiation (Fig. 5*D*), and long-term depression (Fig. 5*E*) all appeared to be indistinguishable in TeNT-expressing versus control mice. Furthermore, whole-cell patch clamp recordings showed that the frequency and amplitude of neuronal mEPSCs were not significantly different between the two groups of animals (Fig. 5*F*). These data indicated that synaptic responses were not globally altered in the astrocyte-specific tetanus toxin-expressing mice, consistent with our in vitro data obtained from hippocampal cultured slices transfected with the lenti-viral vector TeNT$^{\Delta1}$-GFP (Fig. S1 *B* and *C*; Fig. 2 *K*–*M*). Importantly, these results also suggested that there was no leaky expression of tetanus toxin in neuronal cells.

Astrocyte-Specific Expression of TeNT in Vivo Reduced EEG Gamma Power in a Behavioral State-Dependent Manner. To assess the putative effects of astrocyte perturbation on neuronal network activity in vivo, we measured epidural EEG in freely behaving animals. For each mouse, the recording session spanned the entire circadian cycle. The data were analyzed offline to separate three behavioral states: wakefulness, rapid-eye-movement (REM) sleep, and non-REM sleep. We first analyzed the structure and duration of these three states during the light versus the dark phase of the circadian cycle (Fig. 6*A*) and did not find a significant difference between control (2×TG) and 3×TG animals nor between before and after tamoxifen and doxycycline treatments. This suggested that blockade and restoration of astrocytic transmitter release did not alter sleep patterns at the behavioral level.

Next, we measured EEG power spectra for each of the three states in control animals without any treatment (Fig. 6*B*) and characterized typical features for these behavioral contexts (41, 42). We then investigated whether and how EEG power spectra were differentially altered in 3×TG versus control (2×TG) animals under systemic administration of, first, tamoxifen and then doxycycline treatments (Fig. 6 *C*–*E*). In 3×TG animals, when astrocytic transmitter release was blocked by expression of TeNT (3×TG-T), we observed a reduction in EEG power in all

frequency ranges and in all behavioral states (Fig. 6 *C–E*, *Bottom Left*); such an effect could be reversed by doxycycline administration (3×TG-T+D) (Fig. 6 *C–E*, *Upper Right* and *Lower Center*).

Statistical analysis (ANOVA) on measured EEG power spectra revealed that the only significant change associated with induction of TeNT expression was in the low-gamma range (20–40 Hz, maximum ∼30 Hz, Fig. 6*C*, *Upper*) when the animals were awake. During non-REM and REM sleep, however, no significant alteration of the oscillations was observed (Fig. 6 *D* and *E*, *Upper*). Comparison of EEG power spectra before and after doxycycline treatment showed a similar state-dependent spectral modulation in 3×TG mice, but not in control animals (Fig. 6 *C–E*, *Right*).

Astrocyte-Specific TeNT Expression Led to Behavioral Changes in Novel Object Recognition. We then conducted a battery of cognitive tests to investigate if the blockade of astrocytic vesicular release led to behavioral abnormalities. The following paradigms were used (in order of testing sequence): Y-maze, novel object recognition (NOR), and fear conditioning (FC, cued and contextual).

We observed a significant memory deficit in the NOR test (Fig. 7*C*). Wild-type mice naturally spend more time exploring a new object than a familiar one. If a mouse has defective recognition memory, it would be expected to spend equal or more time with a familiar object. The discrimination index [DI = $(T_{NOVEL}-T_{FAMILIAR})/(T_{NOVEL}+T_{FAMILIAR})$] was used to quantify the relative exploration time for the novel versus the familiar object (43). The DI can vary between −1 and +1, where positive scores indicate more time spent with the novel object and a zero or negative score indicates equal or less time spent with the novel object, which would be considered a defective recognition memory (44). Whereas the control (2×TG-T) mice showed significant preference for the novel object, the 3×TG mouse treated with

tamoxifen (3×TG-T, i.e., TeNT expressed in astrocytes) showed a DI value of almost zero, indicating defective recognition memory. However, this defective recognition memory was restored by suppression of TeNT expression by doxycycline feeding (3×TG-T+D), suggesting that gamma oscillations were required for the normal functioning of this type of recognition memory.

In contrast, we found no impairments in Y-maze or FC tests. When mice are tested for navigational working memory using the Y-maze test, they typically prefer to investigate a new arm of the maze rather than return to one that was recently visited. Data were analyzed to determine the number of alternating arm entries without repetition (unique triplets). As shown in Fig. 7*A*, TeNT-expressing mice did not show changes compared with the control groups. Similarly, no significant differences were observed in associative fear memory in a conditioned fear task. In this test, Pavlovian associative learning was evaluated as freezing responses to the conditioned context environment or a previously neutral stimulus (a tone cue) associated with an aversive stimulus (electric foot shock). Freezing levels were very low across all groups in the context test, making group comparisons difficult. Although there was an overall increase in freezing in this trial relative to the habituation trial, no statistically significant group differences were observed. All control and experimental mouse groups exhibited the expected increase in freezing in the conditioned stimulus (CS)+ test upon exposure to the shock-associated cues (Fig. 7*B*).

Discussion

In this study, we used molecular genetic tools to specifically perturb the activity of astrocytes in vitro and in vivo. We induced the expression of TeNT in these cells, taking advantage of the fact that this toxin can efficiently prevent vesicle fusion with the plasma membrane. Using transfected brain slices, we first discovered that vesicular release in astrocytes is required for the maintenance, but not the triggering, of gamma oscillations. Then, using a novel inducible mutant mouse model, we found that TeNT expression in astrocytes reduced EEG power density in the gamma frequency range in vivo. The consistency of findings between different preparations strongly supports the broad and unexpected contribution of astrocytes to gamma oscillatory rhythms, which were previously thought to depend exclusively on neuronal activity. Finally, our results suggest that inhibition of vesicular release in astrocytes and the ensuing disruption of gamma oscillatory activity can profoundly impact cognition, as reflected by the deficit in recognition memory.

Several models of carbachol-induced gamma oscillations in the hippocampus have been previously described (45–47), which postulated a tonic depolarization of excitatory and inhibitory neurons. However, all previously proposed models assumed that such tonic depolarization would have an exclusively neuronal origin and none of them considered the possible involvement of astrocytes. Our results, on the contrary, indicate that intact vesicle trafficking in glial cells is in fact an important part of neuronal network dynamics. Although carbachol-induced depolarization might be sufficient to trigger gamma oscillations, a larger depolarization was required to maintain the oscillatory activity, which could be obtained by recruitment of astrocytes and the consequent release of transmitter from these cells.

Although these data support glutamate as a possible gliotransmitter, our genetic model was not specific in this regard. Sustained TeNT expression in astrocytes can be expected to inhibit the trafficking of all vesicles, potentially blocking the delivery of a variety of channels and transporters to the plasma membrane (48). This could impact the K+ buffering and glutamate uptake functions of astrocytes, which are critical for normal neuronal network dynamics. Similarly, the ability of TeNT expression in astrocytes to affect carbachol-induced oscillations could result from the reduced surface expression of muscarinic
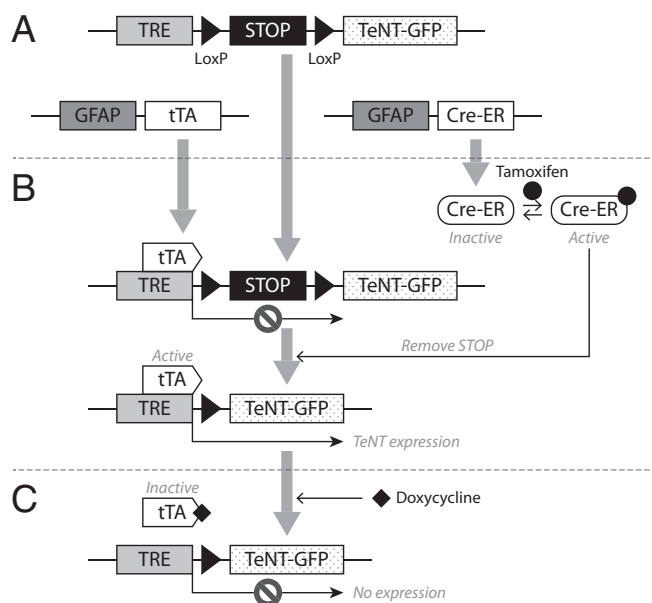
Fig. 4. Genetic constructs used for the generation of the mouse model for temporally and spatially controlled expression of TeNT$^{\Delta1}$-GFP. (*A*) Schematic representation of the 3×TG (triple transgenic) mouse genotype: *GFAP-tTA*; *GFAP-Cre-ERt2*; *TRE-STOP-TeNT-GFP*. (*B*) TeNT is expressed only when the STOP sequence is removed following tamoxifen administration, which activates the Cre-ER protein required to excise the STOP sequence by loxP sequences. (*C*) The tTA is inactivated by doxycycline, resulting in the complete suppression of TeNT expression. Therefore, in the triple transgenic mouse, TeNT toxin expression is induced by tamoxifen injection and suppressed by feeding doxycycline.

Lee et al.
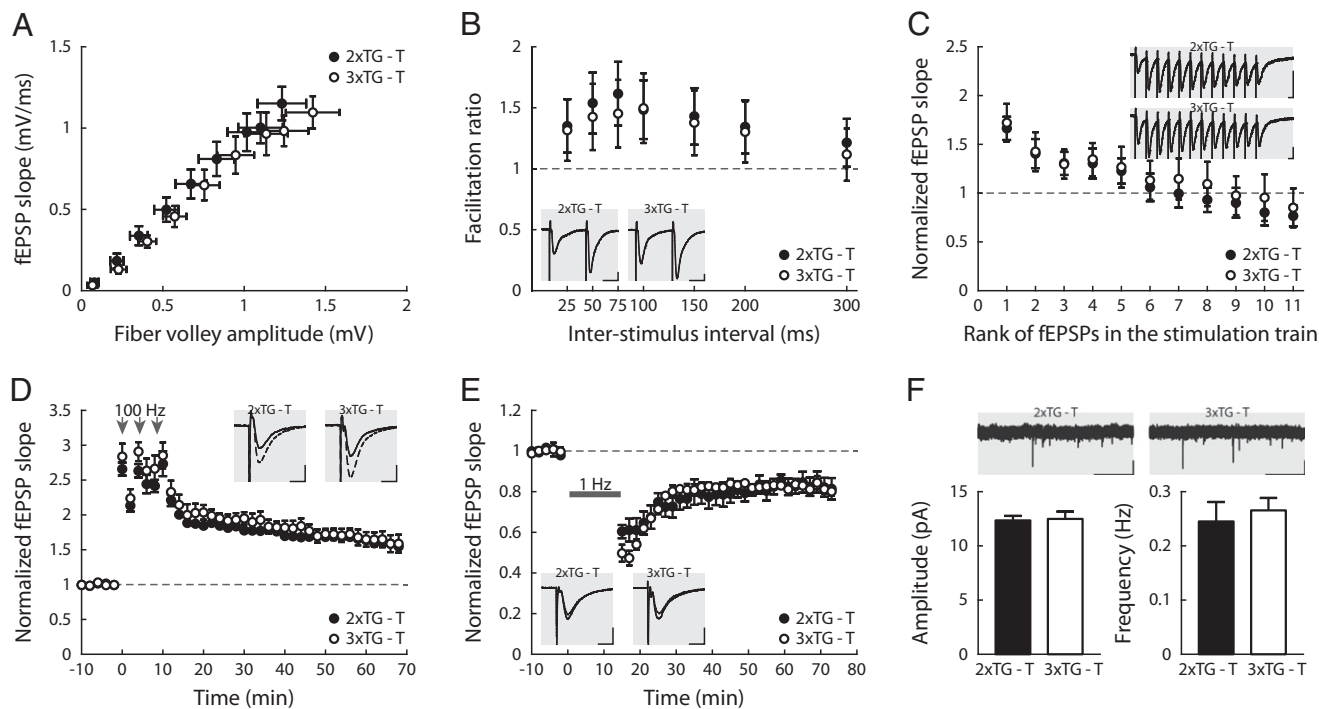
Fig. 5. Synaptic responses were preserved in astrocytic TeNT-expressing transgenic mice. (*A*) Input/output relationship between the fiber volley amplitude and fEPSP slope was determined over a range of stimulus intensities. Each point represents the mean of all slices for each stimulus intensity. Error bar illustrates SEM for both axes (n_{2xTG} = 15 slices from seven mice, n_{3xTG} = 17 slices from eight mice). (*B*) Paired-pulse facilitation induced by two consecutive stimuli (S_1 and S_2) delivered at different time intervals. Facilitation is represented as the S_2/S_1 ratio (one slice per mouse, n = 6 mice each). (*C*) Synaptic fatigue induced by 12 consecutive stimuli at 25-ms interpulse intervals (one slice per mouse, n = 6 mice each). (*D*) Long-term potentiation induced by high frequency (100 Hz for 1 s repeated three times at 5-min intervals, as indicated by the arrows; one slice per mouse, n = 5 mice each). (*E*) Long-term depression induced by low-frequency stimulation (1 Hz for 15 min, n_{2xTG} = 4 slices from three mice, n_{3xTG} = 3 slices from three mice). (*F*) mEPSCs obtained in the presence of TTX (0.5–1 μM) and picrotoxin (100 μM) with demonstrative recordings (*Upper*). (Scale bar, 5 s and 10 pA.) (*Lower*) Mean amplitude/frequency ± SEM. (n_{2xTG} = 14 cells from five mice, n_{3xTG} = 9 cells from three mice). Demonstrative fEPSP traces are illustrated as *Insets* in *B*–*E*. (Scale bar, 10 ms and 0.5 mV.)

acetylcholine receptors, consequent to impaired vesicular trafficking. Although these alternative explanations remain possible, exogenous application of the glutamate receptor agonist AMPA was capable of rescuing the duration of oscillations that were reduced with defective vesicle fusion in our model. Coupled with recent evidence that perisynaptic astrocytes express the vesicular glutamate transporters VGLUT1 and VGLUT3 (49, 50) and that glutamate accumulates in synaptic-like microvesicles in the perisynaptic processes of astrocytes at a concentration comparable to that in synaptic vesicles of excitatory nerve terminals (51), glutamate may be said to in some way mediate the impact of astrocytes on network dynamics.

The fact that the expression of tetanus toxin did not cause evident changes in basal synaptic transmission, as measured in cultured and in acute slices, strongly suggested that the TeNT gene, delivered by lentiviral vectors in slice cultures or integrated into the genome of transgenic mice, was exclusively expressed in astrocytes and not in neurons. Because of their proximity to neuronal synapses, as well as their ability to detect neuronal firing and respond with cytosolic Ca^{2+} elevations, it has been proposed that astrocytes might play an active role in synaptic plasticity (52). Following the induction of TeNT expression, we did not observe appreciable effects on short-term or long-term synaptic plasticity. This is in line with results obtained in a different mouse model in which astrocytic calcium signaling was impaired (14). However, the lack of effect on basal synaptic transmission was in contrast with results obtained in another study using dominant negative SNARE (dnSNARE) mice (33). In the dnSNARE transgenic mouse line, the dnSNARE, amino acids 1–96 of synaptobrevin II, was subcloned under the tetO

promoter, which was silenced by continuous doxycycline feeding from parental mating to 6–8 wk of age. The difference observed between the dnSNARE and our TeNT expression mouse lines might be due to (*i*) different genetic tools used to control the expression of the transgene (continuous doxycycline treatment versus tamoxifen activation), (*ii*) the use of genetically controlled enzymatic degradation of vesicular-release machinery versus controlled expression of a dominant negative peptide, and (*iii*) different levels of expression of the transgene and overall efficiency of vesicular release inhibition in the two systems. It should also be noted that we aimed primarily at controlling possible effects of leaky expression of tetanus toxin in neurons. As such, although our data suggest that synaptic mechanisms were largely intact in our model, protocol-specific contributions of vesicular release to synaptic plasticity cannot be ruled out.

Our in vivo recordings revealed a significant decrease of EEG power density in the low-gamma-frequency range (25–40 Hz) of astrocytic TeNT-expressing mice. The gamma power density reduction was reverted by suppressing the TeNT transgene expression by feeding the animals with doxycycline. Together, these findings demonstrate that TeNT-sensitive vesicular release from astrocytes is required for sustaining gamma oscillations. Interestingly, our results demonstrate that astrocytic TeNT-induced disruption of low gamma oscillations (compared with other frequency ranges) was significant only when the animals were awake, but not during sleep. Such a behavioral state-dependent effect suggests that astrocyte-sustained gamma oscillations could be especially critical for active cognitive functions, such as performance in the novel object recognition test, which evaluates the integrity of recognition memory.
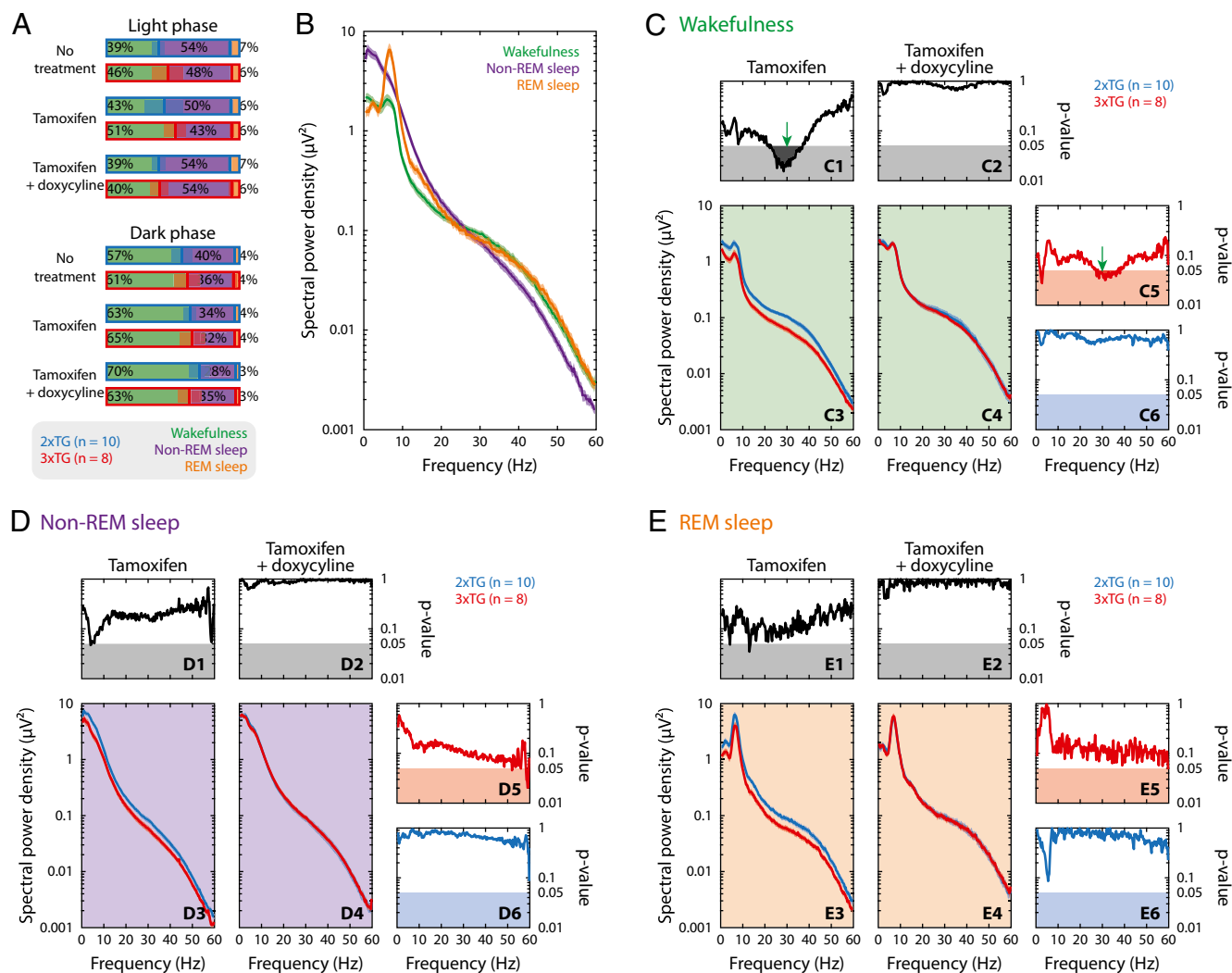
Fig. 6. EEG power spectrum was altered by astrocyte-specific TeNT expression in a behavioral state-dependent manner. (*A*) Percentage of duration of awake (green), non-REM sleep (purple), and REM sleep (orange) during light (*Upper*) and dark (*Lower*) phases for 2xTG (blue, *n* = 10) and 3xTG (red, *n* = 8) under different treatments. Light-colored red and blue horizontal bars represent SD of population. (*B*) Behavioral state-dependent EEG power spectra for control animals (2xTG) without drug treatment. Solid green (awake), purple (non-REM sleep), and orange (REM sleep) curves represent different behavioral states of the animal. Light-colored shades: mean ± SEM (may not be visible because the width of the shade is comparable or less than the thickness of the curves). (*C–E*) Effects of tamoxifen and subsequent doxycycline treatments on EEG power spectra on 3×TG (red) and control (2×TG, blue) animals in awake (*C*), non-REM sleep (*D*), and REM sleep (*E*) state. (*Lower Left*) C3-4, D3-4, and E3-4 show mean (solid curve) and SEM (shade) of power spectra in response to tamoxifen (*Left*) and then doxycycline (*Right*) treatment. (*Upper*) C1-2, D1-2, and E1-2 show ANOVA *P* values between 3×TG and control groups as a function of frequency (solid line); shaded regions at the bottom mark statistical significance (*P* < 0.05). (*Right*) C5-6, D5-6, and E5-6 show ANOVA *P* values of comparison before and after doxycycline treatment for 3×TG (*Upper*: C5, D5, and E5) and control (*Lower*: C6, D6, and E6) animals. The reduction in spectral power density was statistically significant only in low-gamma range (20–40 Hz, green arrows) and only while the animals were awake.

We have used several behavioral tests to investigate the relationship between gliotransmission-dependent gamma oscillations and cognitive functions and behavior. Interestingly, after sequentially testing the same mice in the Y-maze, novel object recognition, and fear conditioning tests, we found that astrocytic TeNT expression resulted in significant deficits in the NOR test, with no differences observed in the Y-maze and fear-conditioning tests. These results indicate that the animals did not have global deficits in attention, sensory functions, or exploratory drive. The deficit in NOR performance, on the other hand, paralleled the alterations in EEG, and like the EEG deficits, it was fully rescued after suppressing the expression of TeNT. Although both the Y-maze task and the NOR test rely on the rodent's innate exploratory behavior in the absence of externally applied positive or negative reinforcement (53), defects were selectively observed in the case of the NOR test. This is partic-

ularly relevant because the Y-maze task evaluates a simpler form of memory processing, i.e., short-term spatial working memory, whereas NOR involves a higher memory load engaging long-term storage, retrieval, and restorage of memory processing (54). During the test phase of the NOR test, a novel object needs to be detected and encoded, whereas the memory trace of a familiar object needs to be updated and reconsolidated after long delays. In contrast, fear conditioning might constitute a strong and highly specific form of learning involving a sympathetic reflex reaction with suppression of voluntary movements (freezing), in which subtle changes in memory content might not be detectable. Moreover, there is strong evidence that suggests fear-conditioned learning encodes a long-term memory process involving the amygdala and the hippocampus (55), whereas the NOR paradigm engages different structures: the hippocampus and adjacent
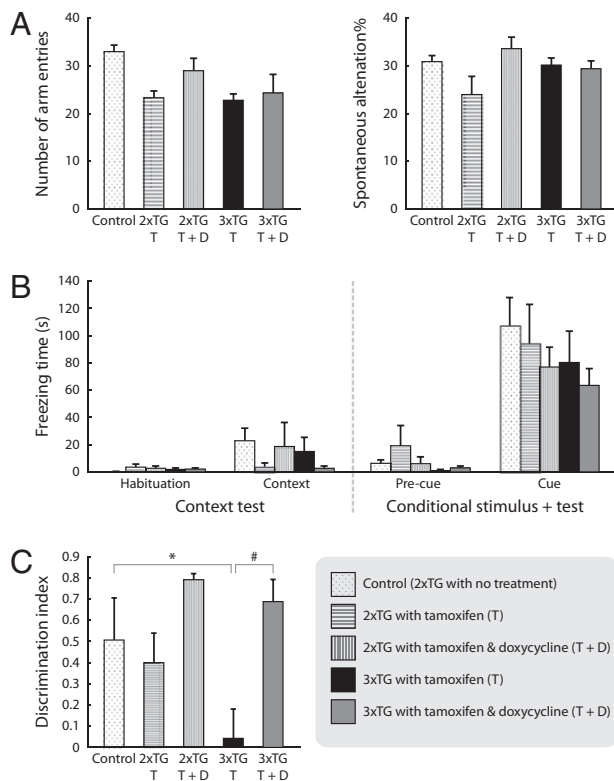
Fig. 7. Astrocyte-specific TeNT expression in vivo provoked a task-specific cognitive decline, manifested as a significant deficit in recognition memory. Y-maze–evaluated (*A*) and FC-evaluated memories (*B*) showed no gamma oscillation-dependent impairments. (*A, Left*) No group differences in general exploratory levels were observed as assessed by the number of arm entries (ANOVA: $F_{(4,17)} = 2.5$, $P = 0.07$). (*A, Right*) Bars represent the percentage of spontaneous alternations (unique triplets) ± SEM. The TeNT-expressing mice (3×TG-T) showed no changes compared with the control groups (ANOVA: $F_{(4,17)} = 2.3$, $P = 0.10$). (*B*) Bars represent the time (in seconds) freezing for animals trained to associate a context or a tone cue with an aversive stimulus (foot shock) ± SEM. The 3×TG-T mice showed similar freezing levels to the control groups in both the contextual (ANOVA: $F_{(4,17)} = 1.0$, $P = 0.41$) and conditioned stimulus tests (ANOVA: $F_{(4,17)} = 1.5$, $P = 0.24$). (*C*) Gamma-oscillation–defective mice suffered a significant memory deficit in a NOR test. Bars represent the discrimination index value [DI = (T_{NOVEL}-$T_{FAMILIAR}$)/(T_{NOVEL}+$T_{FAMILIAR}$)] ± SEM (ANOVA: $F_{(4,17)} = 4.03$, $P = 0.01$). Although the control mice (2×TG, $n_{control} = 5$, $n_{2xTG-T} = 3$, $n_{2xTG-TD} = 3$) showed significant preference for the novel object, the 3xTG-T mice ($n = 5$) did not discriminate between the familiar and the novel object, and therefore these groups were different [Fisher's protected least significant difference (PLSD), $P = 0.02$, labeled with an asterisk]. Such defect was restored in mice with suppression of the TeNT by doxycycline (3xTG-T+D. $n = 6$; Fisher's PLSD, $P = 0.003$, labeled with "#"), suggesting the need for a normal expression of gamma oscillations for the regular processing of recognition memory.

cortical areas including entorhinal, perirhinal, and parahippo-campal cortex (44).

In conclusion, we have shown that astrocytic vesicular release is required for normal cortical gamma oscillations both in vitro and in vivo and that disruption impairs a very specific cognitive function (NOR). These findings demonstrate, to our knowledge for the first time, that fast neural circuit oscillations are tightly regulated by astrocytes. Furthermore, the cognitive and behavioral deficits that we have observed following the disruption of gamma oscillations provide evidence that fast network oscillations are not simply an epiphenomenon of neuronal activity but serve specialized functions that are essential for cognition.

Methods

Groups of one to five mice were housed in standard cages located in individually ventilated racks with ad libitum access to regular food pellets and water (+doxycycline when indicated) in a room with controlled temperature (21 ± 1 °C) and humidity (45–55%) and a 12:12 h light–dark cycle. All animal procedures were in compliance with National Institutes of Health animal care guidelines, and protocols were approved by the Institutional Animal Care and Use Committees of the Salk Institute and The Scripps Research Institute.

Acute Slices and Electrophysiology. Hippocampal slices (350–450 μm thick) were prepared from (*i*) 8- to 12-d-old C57BL/6 mice (and then lentiviral-transfected) or (*ii*) 14- to 17-d-old (TeNT transgenic) mice in sucrose-based ice-cold solutions bubbled with 95% (vol/vol) O_2/5% (vol/vol) CO_2, respectively, containing the following (in mM): (*i*) sucrose, 200; KCl, 1.9; Na_2HPO_4, 1.2; dextrose, 10; $NaHCO_3$, 33; $CaCl_2$, 0.7; $MgCl_2$, 4; ascorbic acid, 0.4; or (*ii*) 110 sucrose, 2.5 KCl, 0.5 $CaCl_2$, 7 $MgCl_2$, 25 $NaHCO_3$, 1.25 NaH_2PO_4, and 10 glucose. The slices were then transferred to artificial cerebrospinal fluid (aCSF) composed of (in mM): (*i*) NaCl, 124; KCl, 5; $CaCl_2$, 2; $MgCl_2$, 2; NaH_2PO_4, 1.2; dextrose, 10; $NaHCO_3$, 33; or (*ii*) 130 NaCl, 2.5 KCl, 1.25 NaH_2PO_4, 24 $NaCHO_3$, 10 glucose, 2 $CaCl_2$, and 1.3 $MgCl_2$, equilibrated with 95% (vol/vol) O_2/5% (vol/vol) CO_2. The tissue was then transiently incubated for 30 min at 32 °C (skipped for transfected slice experiments) and afterward kept at room temperature (24 °C) for ≥1 h before use. Extracellular recordings were obtained using glass microelectrodes filled with aCSF (resistance 2–6 MΩ) in submerged chambers maintained at 32 ± 1 °C (transfected slices) or at room temperature (24 °C, TeNT line). Data were acquired using an Axo-patch 200B amplifier or a Multiclamp 700B and pCLAMP software (Axon Instruments) or the WinLTP program (56).

In experiments involving TeNT mouse line, field-excitatory postsynaptic potentials (fEPSPs) were evoked by stimulation of the Schaffer collateral-commissural fibbers with rectangular 0.2-ms pulses delivered through a concentric bipolar electrode and recorded in the stratum radiatum of the CA1 hippocampal region. Input–output curves were constructed by increasing the stimulation intensity. fEPSPs were evoked each 15 s (0.067 Hz), except for paired-pulse facilitation experiments in which pairs of stimuli (with 25- to 300-ms intervals) were delivered at 0.33 Hz to avoid interferences with slower short-term potentiation (augmentation) or depression processes (57). For long-term potentiation (LTP) and long-term depression (LTD) experiments, fEPSPs were reduced to ~40–60% or 60–80% (10-30 μA stimulation intensity), respectively, and stable baselines of at least 20 min were collected. LTD was induced by low-frequency stimulation (900 stimuli at 1 Hz); LTP was induced by high-frequency stimulation (100 Hz for 1 s repeated three times at 5-min intervals), and the experiments were validated if the fiber volley did not vary significantly. Synaptic fatigue was accessed by 12 consecutive stimuli delivered at 40 Hz.

mEPSCs were recorded at 5 kHz and filtered at 2 kHz from CA1 pyramidal neurons in voltage-clamp mode [voltage holding potential (Vh) = −70 mV] in the presence of TTX (0.5–1 μM) and picrotoxin (100 μM). Events larger than 5 pA were detected using Clampfit software (Molecular Probes). Pipettes had a tip resistance of 4–8 MΩ when filled with internal solution composed of (in mM): 125 K-gluconate, 15 KCl, 8 NaCl, 10 Hepes, 2 EGTA, 10 Tris-phospho-creatine, 4 MgATP, 0.3 GTP (pH 7.25 adjusted with KOH, 292–296 mOsm). Access resistance (typically 15–35 MΩ) was monitored throughout the experiment to ensure stable recordings (<25% variation).

Calcium Imaging. Hippocampal slices were incubated 30–50 min at room temperature in aCSF saturated with 95% (vol/vol) O_2/5% (vol/vol) CO_2 and containing 10 μM Fura2-AM (Molecular Probes). For imaging calcium dynamics in astrocytes/HEK cocultures, cells were incubated 30 min in aCSF containing 3 μM Fura2-AM and 0.02% Pluronic F-127. Samples were excited with a xenon lamp, and the excitation wavelengths (350 and 380 nm) were selected using a polychromatic illumination system (TILL Photonics). Emission images (510 nm) were acquired using a cooled CCD camera (MicroMax; Princeton Instruments) and the Axon Imaging Workbench software (Axon Instruments). Glial cells were mechanically stimulated using patch pipettes (1–2 MΩ tip resistance) mounted on a patch clamp headstage controlled by a micromanipulator. Stimulation was accomplished by approaching the cell with the tip of the microelectrode while monitoring the tip resistance. Using this protocol, responses were elicited when the pipette was in close enough proximity to increase tip resistance to 15–20 MΩ, which did not result in membrane rupture.

Slice Cultures. Horizontal hippocampal slices (400 μm thick) were cut from P9 mouse pups (C57BL/6) in ice-cold calcium-free minimum essential medium

(MEM) containing 11 mM MgSO$_4$. Immediately after cutting, the slices were transferred on 0.4-μm Millicell-CM membrane inserts (Millipore) at the interface between culture media and air. Culture media contained: 50% Basal Medium Eagle; 25% Earle's Balanced Salt Solution; 25 mM Hepes-NaOH, pH 7.20; 6.5 mg/mL glucose; 100 μg/mL streptomycin; and 25% horse serum. Slices were kept in a humidified incubator at 35 °C in 5% CO$_2$. After the first 3 d, the slices were transferred to medium containing 5% horse serum. Medium was changed every 3 d. Extracellular recordings were made as described for acute slices, and intracellular recordings were made using glass electrodes (resistance 5–8 MΩ) filled with (in mM): 121.5 potassium gluconate, 17.5 KCl, 9 NaCl, 1 MgCl$_2$, 10 Hepes-NaOH (pH 7.2), 2 Mg-ATP, 0.5 Li-GTP, except for mEPSCs recordings, in which case the following intracellular solution was used (composition in mM): CsCl, 140; NaCl, 4; CaCl$_2$, 0.5; EGTA, 5; Hepes, 10; Na-GTP, 0.5; Mg-ATP, 2; adjusted to pH 7.33 with CsOH; 295 mOsm. mEPSCs were recorded at 5 kHz in voltage-clamp mode [Vh = −70 mV in the presence of TTX (0.5–1 μM) and bicuculline (10 μM)]. Access resistance (typically 15–35 MΩ) was monitored throughout the experiment to ensure stable recordings (<25% variation).

Lentiviral Vectors. The human promoter of the glial fibrillary acidic protein gene (provided by M. Brenner) was digested with the restriction enzymes ClaI and AgeI and cloned into a lentiviral vector[24,25] digested with the same enzymes. This construct was used to generate the Lenti-hGFAP-GFP viral vector. The TeNT and GFP genes were ligated together following PCR mutagenesis to create compatible ends. It was empirically determined that only the fusion protein containing a truncated TeNT (TeNT$^{\Delta1}$, in which the last 12 amino acids are missing) is both catalytically active and green fluorescent. The TeNT$^{\Delta1}$-GFP chimera was digested with AgeI and SmaI and cloned in the compatible ends in the Lenti-hGFAP vector. Vector particles were produced as described (58, 59). Titers >5 × 10^9 transduction units/mL were routinely achieved, as determined by p24 ELISA quantitation (Alliance; DuPont-NEN).

Immunofluorescence. Slices were fixed in 4% paraformaldehyde for 2 h at room temperature. Following several washes in TBS buffer (Tris·HCl, pH 7.40, NaCl 150 mM), slices were permeabilized and blocked overnight at 4 °C in TBST (TBS with 0.1% Triton X-100) containing 5% normal donkey serum. The monoclonal anti-NeuN (Chemicon, 1:250) and rabbit polyclonal anti-GFAP (DAKO, 1:400) were added directly to the permeabilizing/blocking solution and incubated with the slices for 2 d at 4 °C. The slices were then washed for 24 h in TBS at 4 °C. The last wash was done in TBST for 1 additional hour. The anti-mouse IgM-Cy5–conjugated (Jackson, 1:250) and anti-rabbit IgG-Cy3–conjugated (Jackson, 1:250) purified antibodies were added to the TBST. Following 24 h incubation at 4 °C, the slices were washed for 24 h in TBS at 4 °C and mounted. Images were acquired using a Zeiss laser scanning microscope equipped with Ar/Kr and HeNe$_2$ laser sources.

Triple Transgenic Mouse. The translational and transcriptional STOP sequence flanked by loxP (1.3 kbp) were obtained from the clone CVU51223 (GenBank accession no. U51223.1) (32) and subcloned into pTRE-Tight vector (Clontech). pTRE-Tight contains a multiple cloning site (MCS) immediately downstream of the Tet-responsive Ptight promoter. Ptight contains a modified Tet response element (TRE$_{mod}$), which consists of seven direct repeats of a 36-bp sequence that contains the 19-bp tet operator sequence (tetO). The TRE$_{mod}$ is just upstream of the minimal CMV promoter, which lacks the enhancer that is part of the complete CMV promoter. Consequently, Ptight is silent in the absence of binding of TetR or the tetO sequences. The same TeNT$^{\Delta1}$-GFP gene used in the lentiviral vector was excised and subcloned into the pTRE-Tight vector after the STOP sequence with loxP sequence. Whole transgene including tetO-loxP-STOP-loxP-TeNT$^{\Delta1}$-GFP-SV40 polyA was excised by XhoI and injected into mouse embryos to generate the transgenic mouse lines. The founder mice were crossed with C57BL/6 mice for several generations before the examination of the TeNT expression profile. The optimal tamoxifen treatment was 2 × 100 mL (10 mg/mL) injections (24 h apart), and the transcriptional level of TeNT-GFP peaked 2 d after the last injection. The transcript of the toxin was no longer detectable 3 d after the transgene was turned off by feeding the mouse doxycycline (0.05 mg/mL in drinking water).

In Vivo EEG. Mice were placed in a stereotaxic apparatus under isoflurane anesthesia (1–2%). A midsaggital incision was then made on the shaved scalp disinfected with ethanol and betadine to expose the skull. Stainless steel screw electrodes were implanted for chronic EEG recordings. Differential recordings were made between two electrodes placed in the frontal and parietal bones [−2.06 mm along the antero-posterior (AP) axis and 1.5 mm along the medio-lateral (ML) axis referenced to bregma (60)], and

a third electrode was placed over cerebellum as ground. Two additional wire electrodes were placed in the cervical musculature for electromyogram (EMG) recordings of postural tone. Insulated leads from these electrodes were then soldered to a miniconnector cemented to the skull with dental acrylic. The wound was sutured and treated with antibiotic ointment, and the animal was injected s.c. with flunixin (analgesic).

One week after surgery, animals were treated during 2 consecutive days with a single (i.p.) injection of tamoxifen (100 mL, 10 mg/mL). Recording sessions were performed 3 d after the second injection. Animals were first habituated in individual recording chambers for 48 h under standard temperature and light/dark cycle conditions. Then the animals were recorded continuously for 24 h starting after light onset. The EEG and EMG signals were amplified by a Grass Model 7D polygraph, filtered in a frequency range of 0.3–60 Hz, sampled at 256 Hz, and stored on a hard drive downsampled to 128 Hz for offline analysis, using software supplied by Kissei Comptec. Fifteen-second epochs of the polygraphic recordings were semiautomatically classified into three behavioral states: wakefulness, REM sleep, and non-REM sleep. Spectral analysis of EEG signals was performed by using fast Fourier transform on 4-s epochs and 1-Hz frequency bins. Epochs contaminated with artifacts as well as those occurring at transitions between behavioral states were discarded from analyses. For each behavioral state, i.e., wakefulness, REM sleep, and non-REM sleep, two-way ANOVA was applied to spectral power density at each frequency bin for the estimated power spectra. The first independent factor was genotype (2x versus 3x) and the second factor was treatment (tamoxifen versus tamoxifen+doxycycline). A significance level of $P = 0.05$ was used to identify frequency ranges in which marked differences in EEG power were observed between the two genotypes as well as between the two treatments.

Y-Maze. Spontaneous alternation, the tendency to alternate free choices in a Y-maze (three arms), was used to study working memory. A single 5-min test was performed in which each mouse was placed in the center of the Y. Total number of arm entries and the order of entries were determined from video-recorded sessions. Spontaneous alternations were defined as consecutive triplets of different arm choices (typical score for normal mice was 60–70%).

NOR. The NOR test assesses the ability to recognize a novel object in the environment. Adapted from Benice and colleagues (61, 62), mice were individually habituated to a 51- × 51- × 39-cm open field for 5 min. For the familiarization trials, two plastic toy objects were placed in the open field (one in each of two corners), and an individual animal was allowed to explore for 5 min. This was repeated another four times (1-min intertrial interval). Two weeks later, each mouse was tested in a NOR test in which a novel object replaced one of the familiar objects (no preference for any object was observed in pilot studies using C57BL/6J mice). All objects (fixed to 10- × 7- × 0.5-cm clear Plexiglas bases to prevent displacement) and the arena were thoroughly cleaned with 70% ethanol between trials to remove odors. "Exploration" was defined as approaching the object nose first within 2–4 cm. The numbers of approaches toward each object were calculated for each trial. Habituation to the objects across the five familiarization trials (decreased contacts) is an initial measure of learning, and renewed interest (increased contacts) in the new object indicates evidence of object memory.

Cued and Contextual Fear Conditioning. Conditioning took place inside sound-proofed boxes with a Mouse NIR Video Fear Conditioning System (Med Associates). The conditioning chambers (26 × 26 × 17 cm) are made of Plexiglas with speakers and lights mounted on two opposite walls and a shockable grid floor.

On day 1, mice were placed in the conditioning chamber for 5 min to habituate them to the apparatus. On day 2, the mice were exposed to the context and CS (30 s, 3,000 Hz, 80 dB sound + white light) in association with foot shock (0.60 mA, 2-s, scrambled current). In each session, the mice received three shock exposures, each in the last 2 s of a 30-s tone/light exposure. Two weeks later, contextual conditioning (as determined by freezing behavior) was measured in a 5-min test in the chamber where the mice were trained (context test). On the following day, the mice were tested for cued conditioning (CS+ test). The mice were placed in a novel context (white opaque plastic floor and walls creating a circular compartment, in contrast to a clear plastic square compartment and metal grid floor) for 3 min and then exposed to the CS for 3 min. Freezing behavior (absence of all voluntary movements except breathing) was measured in all sessions by real-time digital video recordings calibrated to distinguish between subtle movements (whisker twitch, tail flick) and freezing behavior. Freezing behavior in the context and cued tests (relative to the same context before shock and an altered context before tone, respectively) was indicative of the formation of an association between the particular stimulus (environment or CS) and the shock.

1. Başar-Eroglu C, Strüber D, Schürmann M, Stadler M, Başar E (1996) Gamma-band responses in the brain: A short review of psychophysiological correlates and functional significance. *Int J Psychophysiol* 24(1-2):101–112.
2. Herrmann CS, Demiralp T (2005) Human EEG gamma oscillations in neuropsychiatric disorders. *Clin Neurophysiol* 116(12):2719–2733.
3. Whittington MA, Traub RD, Jefferys JG (1995) Synchronized oscillations in interneuron networks driven by metabotropic glutamate receptor activation. *Nature* 373(6515):612–615.
4. Penttonen M, Kamondi A, Acsády L, Buzsáki G (1998) Gamma frequency oscillation in the hippocampus of the rat: Intracellular analysis in vivo. *Eur J Neurosci* 10(2):718–728.
5. Buhl DL, Harris KD, Hormuzdi SG, Monyer H, Buzsáki G (2003) Selective impairment of hippocampal gamma oscillations in connexin-36 knock-out mouse in vivo. *J Neurosci* 23(3):1013–1018.
6. Zlomuzica A, et al. (2010) Deletion of connexin45 in mouse neurons disrupts one-trial object recognition and alters kainate-induced gamma-oscillations in the hippocampus. *Physiol Behav* 101(2):245–253.
7. Verkhratsky A, Rodríguez JJ, Parpura V (2012) Calcium signalling in astroglia. *Mol Cell Endocrinol* 353(1-2):45–56.
8. Fiacco TA, Agulhon C, McCarthy KD (2009) Sorting out astrocyte physiology from pharmacology. *Annu Rev Pharmacol Toxicol* 49:151–174.
9. Halassa MM, Fellin T, Haydon PG (2009) Tripartite synapses: Roles for astrocytic purines in the control of synaptic physiology and behavior. *Neuropharmacology* 57(4):343–346.
10. Santello M, Calì C, Bezzi P (2012) Gliotransmission and the tripartite synapse. *Adv Exp Med Biol* 970:307–331.
11. Cornell-Bell AH, Finkbeiner SM, Cooper MS, Smith SJ (1990) Glutamate induces calcium waves in cultured astrocytes: Long-range glial signaling. *Science* 247(4941):470–473.
12. Wenker I (2010) An active role for astrocytes in synaptic plasticity? *J Neurophysiol* 104(3):1216–1218.
13. Henneberger C, Papouin T, Oliet SH, Rusakov DA (2010) Long-term potentiation depends on release of D-serine from astrocytes. *Nature* 463(7278):232–236.
14. Agulhon C, Fiacco TA, McCarthy KD (2010) Hippocampal short- and long-term plasticity are not modulated by astrocyte Ca2+ signaling. *Science* 327(5970):1250–1254.
15. Gray CM (1994) Synchronous oscillations in neuronal systems: Mechanisms and functions. *J Comput Neurosci* 1(1-2):11–38.
16. Wang XJ (2010) Neurophysiological and computational principles of cortical rhythms in cognition. *Physiol Rev* 90(3):1195–1268.
17. Fisahn A, Pike FG, Buhl EH, Paulsen O (1998) Cholinergic induction of network oscillations at 40 Hz in the hippocampus in vitro. *Nature* 394(6689):186–189.
18. Fellous JM, Sejnowski TJ (2000) Cholinergic induction of oscillations in the hippocampal slice in the slow (0.5-2 Hz), theta (5-12 Hz), and gamma (35-70 Hz) bands. *Hippocampus* 10(2):187–197.
19. Parpura V, et al. (1994) Glutamate-mediated astrocyte-neuron signalling. *Nature* 369(6483):744–747.
20. Bezzi P, et al. (1998) Prostaglandins stimulate calcium-dependent glutamate release in astrocytes. *Nature* 391(6664):281–285.
21. Liu T, et al. (2011) Calcium triggers exocytosis from two types of organelles in a single astrocyte. *J Neurosci* 31(29):10593–10601.
22. Araque A, Li N, Doyle RT, Haydon PG (2000) SNARE protein-dependent glutamate release from astrocytes. *J Neurosci* 20(2):666–673.
23. Eisel U, et al. (1993) Tetanus toxin light chain expression in Sertoli cells of transgenic mice causes alterations of the actin cytoskeleton and disrupts spermatogenesis. *EMBO J* 12(9):3365–3372.
24. Schiavo G, Matteoli M, Montecucco C (2000) Neurotoxins affecting neuroexocytosis. *Physiol Rev* 80(2):717–766.
25. Pasti L, Zonta M, Pozzan T, Vicini S, Carmignoto G (2001) Cytosolic calcium oscillations in astrocytes may regulate exocytotic release of glutamate. *J Neurosci* 21(2):477–484.
26. Yu X, Duan KL, Shang CF, Yu HG, Zhou Z (2004) Calcium influx through hyperpolarization-activated cation channels (I(h) channels) contributes to activity-evoked neuronal secretion. *Proc Natl Acad Sci USA* 101(4):1051–1056.
27. Engel AK, Fries P, Singer W (2001) Dynamic predictions: Oscillations and synchrony in top-down processing. *Nat Rev Neurosci* 2(10):704–716.
28. Zhang Q, et al. (2004) Fusion-related release of glutamate from astrocytes. *J Biol Chem* 279(13):12724–12733.
29. Brenner M, Kisseberth WC, Su Y, Besnard F, Messing A (1994) GFAP promoter directs astrocyte-specific expression in transgenic mice. *J Neurosci* 14(3 Pt 1):1030–1037.
30. Lois C, Hong EJ, Pease S, Brown EJ, Baltimore D (2002) Germline transmission and tissue-specific expression of transgenes delivered by lentiviral vectors. *Science* 295(5556):868–872.
31. Gossen M, et al. (1995) Transcriptional activation by tetracyclines in mammalian cells. *Science* 268(5218):1766–1769.
32. Sauer B (1993) Manipulation of transgenes by site-specific recombination: Use of Cre recombinase. *Methods Enzymol* 225:890–900.
33. Pascual O, et al. (2005) Astrocytic purinergic signaling coordinates synaptic networks. *Science* 310(5745):113–116.
34. Hirrlinger PG, Scheller A, Braun C, Hirrlinger J, Kirchhoff F (2006) Temporal control of gene recombination in astrocytes by transgenic expression of the tamoxifen-inducible DNA recombinase variant CreERT2. *Glia* 54(1):11–20.
35. Feil R, Wagner J, Metzger D, Chambon P (1997) Regulation of Cre recombinase activity by mutated estrogen receptor ligand-binding domains. *Biochem Biophys Res Commun* 237(3):752–757.
36. Metzger D, Chambon P (2001) Site- and time-specific gene targeting in the mouse. *Methods* 24(1):71–80.
37. Leone DP, et al. (2003) Tamoxifen-inducible glia-specific Cre mice for somatic mutagenesis in oligodendrocytes and Schwann cells. *Mol Cell Neurosci* 22(4):430–440.
38. Barton MD, et al. (2002) Modified GFAP promoter auto-regulates tet-activator expression for increased transactivation and reduced tTA-associated toxicity. *Brain Res Mol Brain Res* 101(1-2):71–81.
39. Su M, et al. (2004) Expression specificity of GFAP transgenes. *Neurochem Res* 29(11):2075–2093.
40. Casper KB, McCarthy KD (2006) GFAP-positive progenitor cells produce neurons and oligodendrocytes throughout the CNS. *Mol Cell Neurosci* 31(4):676–684.
41. Huber R, Deboer T, Tobler I (2000) Effects of sleep deprivation on sleep and sleep EEG in three mouse strains: Empirical data and simulations. *Brain Res* 857(1-2):8–19.
42. Franken P, Malafosse A, Tafti M (1998) Genetic variation in EEG activity during sleep in inbred mice. *Am J Physiol* 275(4 Pt 2):R1127–R1137.
43. Ennaceur A (1998) Effects of lesions of the Substantia Innominata/Ventral Pallidum, globus pallidus and medial septum on rat's performance in object-recognition and radial-maze tasks: Physostigmine and amphetamine treatments. *Pharmacol Res* 38(4):251–263.
44. Antunes M, Biala G (2012) The novel object recognition memory: Neurobiology, test procedure, and its modifications. *Cogn Process* 13(2):93–110.
45. Traub RD, et al. (2000) A model of gamma-frequency network oscillations induced in the rat CA3 region by carbachol in vitro. *Eur J Neurosci* 12(11):4093–4106.
46. Tiesinga PH, José JV (2000) Robust gamma oscillations in networks of inhibitory hippocampal interneurons. *Network* 11(1):1–23.
47. Akay M, Wang K, Akay YM, Dragomir A, Wu J (2009) Nonlinear dynamical analysis of carbachol induced hippocampal oscillations in mice. *Acta Pharmacol Sin* 30(6):859–867.
48. Galli T, et al. (1994) Tetanus toxin-mediated cleavage of cellubrevin impairs exocytosis of transferrin receptor-containing vesicles in CHO cells. *J Cell Biol* 125(5):1015–1024.
49. Ormel L, Stensrud MJ, Bergersen LH, Gundersen V (2012) VGLUT1 is localized in astrocytic processes in several brain regions. *Glia* 60(2):229–238.
50. Ormel L, Stensrud MJ, Chaudhry FA, Gundersen V (2012) A distinct set of synaptic-like microvesicles in atroglial cells contain VGLUT3. *Glia* 60(9):1289–1300.
51. Bergersen LH, et al. (2012) Immunogold detection of L-glutamate and D-serine in small synaptic-like microvesicles in adult hippocampal astrocytes. *Cereb Cortex* 22(7):1690–1697.
52. Jourdain P, et al. (2007) Glutamate exocytosis from astrocytes controls synaptic strength. *Nat Neurosci* 10(3):331–339.
53. Ennaceur A, Delacour J (1988) A new one-trial test for neurobiological studies of memory in rats. 1: Behavioral data. *Behav Brain Res* 31(1):47–59.
54. Ennaceur A (2010) One-trial object recognition in rats and mice: Methodological and theoretical issues. *Behav Brain Res* 215(2):244–254.
55. Bienvenu TC, Busti D, Magill PJ, Ferraguti F, Capogna M (2012) Cell-type-specific recruitment of amygdala interneurons to hippocampal theta rhythm and noxious stimuli in vivo. *Neuron* 74(6):1059–1074.
56. Anderson WW, Collingridge GL (2007) Capabilities of the WinLTP data acquisition program extending beyond basic LTP experimental functions. *J Neurosci Methods* 162(1-2):346–356.
57. Zucker RS, Regehr WG (2002) Short-term synaptic plasticity. *Annu Rev Physiol* 64:355–405.
58. Zufferey R, et al. (1998) Self-inactivating lentivirus vector for safe and efficient in vivo gene delivery. *J Virol* 72(12):9873–9880.
59. Dull T, et al. (1998) A third-generation lentivirus vector with a conditional packaging system. *J Virol* 72(11):8463–8471.
60. Paxinos G, Franklin KBJ, Franklin KBJ (2001) *The Mouse Brain in Stereotaxic Coordinates* (Academic Press, San Diego), 2nd Ed.
61. Benice TS, Lou JS, Eaton R, Nutt J (2007) Hand coordination as a quantitative measure of motor abnormality and therapeutic response in Parkinson's disease. *Clin Neurophysiol* 118(8):1776–1784.
62. Benice TS, Raber J (2008) Object recognition analysis in mice using nose-point digital video tracking. *J Neurosci Methods* 168(2):422–430.